Flood Modelling Using Integration of Multi-data Analysis and HEC-RAS Model in Mata Allo River, Sulawesi

Uca[1*], *Mustari* Lamada[2], *Amal* Arfan[1], and *Nurul Afdal* Haris[3]

[1]Department of Geography, Faculty of Mathematics and Natural Sciences, Makassar State University, 90244 Indonesia
[2]Informatics and Computer Engineering, Faculty of Engineering, Makassar State University, 90244 Indonesia
[3]Master in Remote Sensing, Faculty of Geography, Gadjah Mada University, 55281, Indonesia

Abstract. The amount of rainfall in a watershed with steep slopes, small cross-sectional areas, and less water catchment areas. This will cause an increase in water discharge in the river which can cause flooding. These characteristics can be found in Mata Allo River, Enrekang Regency. To identify the most flood-hit areas, the simulating model can be done utilizing the HEC-RAS program. Use of Satellite Imagery Data such as Sentinel-2 for extracting land use data information, and Sentinel-1 for data extraction of actual water bodies/rivers. The analysis is carried out by integrating the interpretation results from multi-sensor images with the results of modeling the flood inundation area using HEC-RAS. Based on the analysis results, the land use classification accuracy is 82.9% for Sentinel-2 data using the random forest algorithm. While for the actual extraction of water bodies using Sentinel-1 imagery was 89.6%. Approaching the threshold value between water and non-water bodies is taken using -13.39. The inundation area in the study area reached 87.66ha at the largest discharge model. The most affected land use after integrating each data is built-up land, most of which are settlements covering an area of 47.26ha.

1 Introduction

The territory of Indonesia is located in a wet tropical climate zone with quite high rainfall [1]. If detailed, about 80 percent of disasters in Indonesia are classified as hydrometeorological disasters such as floods, landslides, and hurricanes. Floods require serious attention from various parties because they contribute 37 percent of 143 of all disasters that occur nationally [2]. Floods occur when the volume of water flowing in drainage channels or rivers exceeds the flow capacity and absorption capacity of the surrounding dry land [3], [4]. Every year, the intensity and area of flood areas continue to increase due to environmental damage caused by humans, so the surface runoff rate increases, and the area of water catchment area decreases, which almost occurs in all watersheds in Indonesia. [5], [6]. One of the efforts to reduce the risk of flood disasters is flood spatial data management. With spatial flood information, decision-making in spatial planning for affected areas will be easier.

The Mata Allo River which passes through Enrekang Regency is one of the contributors to floodwater runoff yearly when there is an increase in rain intensity [7]. One of the causes of this flood is the change in land use in the upstream area of the river [8]. The area that is always affected is the City of Enrekang in the Juppandang district. Almost every year the area experiences floods with different flood intensities. One of the major flood events occurred on April 29, 2019, which caused the City of Enrekang to be flooded [2].

Spatial modeling in mapping flood hazard and vulnerability simulating the coverage of inundation areas and their potential impacts [9]. Integrating spatial data, such as remote sensing data [10] is widely used, because the additional information obtained from remote sensing data will strengthen the results and sharpen the spatial information of the analysis results carried out [11]–[13]. The lack of spatial data that provides information about the condition of the area that has the potential to be affected by flooding will cause gradual losses when a flood disaster occurs again. So that a need for spatial information on flood disaster areas that can be a reference or reference in disaster mitigation activities. Seeing the dynamics of the development of hydrological studies, especially on the phenomenon of urban flooding, now the development of the study is leading to a spatial (spatial) based study. Spatial-based studies cannot be separated from the role of Geographic Information Systems (GIS) as a supporting tool.

Moreover, the function of GIS can present a form of modeling of a hydrological phenomenon and the phenomenon of flooding in urban areas [14], [15]. Spatial modeling can be done by utilizing Geographic Information Systems (GIS) and Remote Sensing (RS) as information providers in the spatial modeling input. One of the programs in flood modeling is the HEC-RAS program. Using this program, the flood inundation area can be simulated based on the river discharge at the time of the flood [16], [17].

In this study, we approach the integration of multi-sensor images (optical and radar) on flood modeling

* Corresponding author: ucasideng@unm.ac.id

results by utilizing DEM data and river discharge results from field measurements during flood events using the HEC-RAS program.

2 Methods

2.1 Study Area

The location of the flood modeling is in Juppandang Village, Enrekang District, Enrekang Regency. Astronomically at 3°33'17.22" S - 3°34'23.81" S and 119°45'59.91" E - 119°47'14.10" E. In this area, there is the Mata Allo River, where on the west side there is an urban center that is densely populated with settlements. The residential area is flood-prone every year when rainfall increases [2]. More details can be seen on the following map.

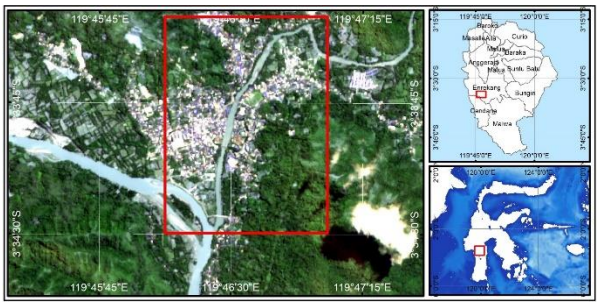

Fig. 1. Research Location Map

2.2 Data Used

This study uses two types of images, radar images, and optical images. For radar images, use Sentinel-1 Image and Sentinel-2 for optical images. The image can be obtained at https://scihub.copernicus.eu/dhus/#/home. In addition, DEM (Digital Elevation Model) data is also prepared for flood analysis. These data can be obtained from DEMNAS Indonesia with an 8.2m resolution at https://tanahair.indonesia.go.id/demnas (specifically for the Indonesian region). For more details regarding the details of data usage, see the following table,

Table 1. Description of the data used

No	Data	Utility
1	Sentinel-2 image, 10m resolution (Bands 2,3,4,8) Recorded May 5, 2019, Type S2MSI2A, Sensing Orbit Descending, Cloud Coverage on scene 19,733.	Extraction of land cover information
2	Sentinel-1 image, 10m resolution (VV Polarization) Recording April 27, 2019, Product Type Ground Range Detected (GRD), Interferometric Wide swath (IW), VH-VV Polarization, Sensing Orbit Descending	Extraction of actual water body(river) information
3	DEM, DEMNAS 0.27arcsecond/8.2m resolution	Modeling Terrain data for the study area for flood modeling, extracting cross-sectional data for river flow for water level models
4	Google Earth Images	Used in the interpretation of land use when making samples for testing the accuracy of classification results using Sentinel 2 imagery

Based on information on flood events by the National Disaster Management Agency in Enrekang Regency. April 29, 2019, was recorded as one of the major flood events in Enrekang Regency. Therefore, this study tries to simulate and model the flooding that occurred on that date. By utilizing sentinel-2, sentinel-1, and DEM images to determine the affected area.

2.3 Data Analysis

Data analysis for Radar Images and optical images, both use the SNAP program as the default analysis program. Can be downloaded at https://step.esa.int/. As for the DEM data in modeling flood discharge, the whole is carried out on the HEC-RAS program (can be obtained at https://www.hec.usace.army.mil/).

Before analyzing each of the data used. First, for the image data, both sentinel-2 and sentinel-1, corrections are made to improve the existing data. For Sentinel-2 data itself, corrections are made such as reprojection to match the Sentinel-1 data, and Rayleigh correction to reduce bias in the atmosphere. Meanwhile, the atmospheric correction was not carried out, because the data obtained had gone through the TOA (Top of Atmosphere) to BOA (Bottom of Atmosphere) process. For Sentinel-1 data itself, special corrections are needed, such as applying the Apply Orbit File to update the metadata on the image because the metadata of Sentinel-1 products is generally less accurate [18]. Then apply Thermal Noise Removal to reduce noise. Calibration to produce sigma band output on either VV or VH polarization data (depending on the data used). Furthermore, Terrain Correction involves DEM and orbit files to correct errors from the SAR system such as layover, shadow, and foreshortening. So that the geometric representation of the image corresponds to the field coordinates. And converting data from sigma naught (σ°) to Digital Number (DN) which is in units of decibel (dB) as a backscattering coefficient. And lastly, subset or cut the image to fit the scope of the study area. At the same time reducing the computational load [10].

For a more complete analysis procedure, see the diagram of the data analysis process below.

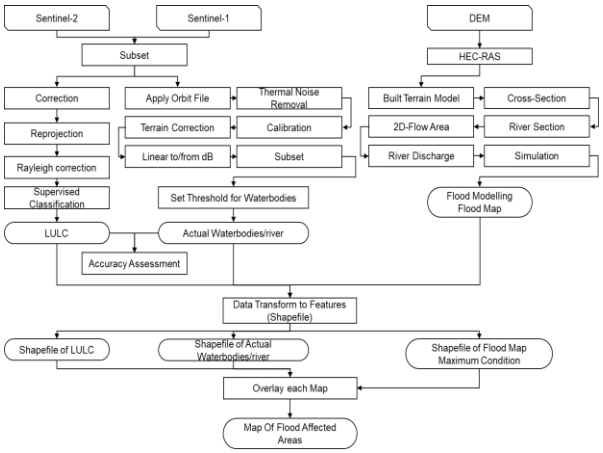

Fig. 2. Analysis flow chart

Land use classification uses the Random Forest method which is included in the Supervised Classification system. Based on the ability of the Random Forest algorithm to take into account all aspects of input and computation that are repeated as needed [19]. to produce more accurate classification results, both are used for the classification of diverse land cover [10], [20], [21].

Extraction of water bodies using radar imagery [22] by setting limits or thresholds on backscattering values [23]–[25]. By determining the value boundary between water bodies and non-water bodies, it will be easier when the extraction process is actual water bodies or rivers. The date of recording the image used is also the dry phase for paddy farming. so that it will not interfere with the actual extraction of water bodies.

Modeling using the HEC-RAS program goes through several stages. Such as making Terrain data from DEM data which is used as the basis for forming a river cross-section model and the elevation of the study area. make cross-section data along the study river, to find out the 2D cross-sectional model. So that at the time of flood modeling with river discharge input, it is known that the increase in river water level occurred [17].

3 Results

3.1 Data Visualization

Utilization of Remote Sensing data with different sensors such as optics and radar is very helpful in analyzing land cover to disasters [26]–[28]. In this study, Sentinel-2 and Sentinel-1 data are used, as optical sensors and radar sensors. In land cover data visualization for interpretation purposes, it is enough to use TrueColor Composite [29], this is because, at the study location, it is quite clear that the differences between each object are visible. For Sentinel-1 data using VV polarization due to the extraction of water bodies [30], not paying too much attention to Horizontal scattering as for land use. So the use of VV Polarization will be more optimal for the extraction of water bodies [13]. Meanwhile, the DEM data which is converted into Terrain Model is intended to facilitate the determination of River Reach [31] or the main flow of the Mata Allo River, and the determination of the Bank as the left and right boundary of the river. The appearance of the data used can be seen in **Figure 3** below,

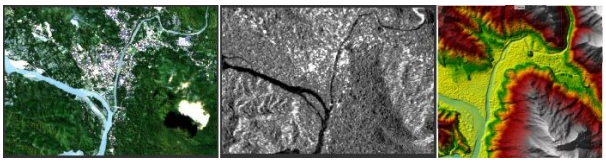

Fig. 3. Data used in the analysis, Sentinel-2 RGB (*left*), Sentinel-1 Polarized VV (*mid*), DEM (Terrain Model) (*Right*)

3.2 Waterbodies Extraction

Analysis using Sentinel-1 Image data by utilizing VV polarization. Extraction of water bodies is carried out by determining the boundary value between the backscatter value of water objects and non-water objects [23], [24]. Based on the backscattering curve value, it was found that the water body value was below -13.39dB (**Figure 4**). The results of determining the limit or threshold, it is then applied to separate the backscatter value of water objects. So that the data is obtained as shown in **Figure 5**. This method is a fairly efficient way of extracting water bodies [22] by exploiting the backscattering response of the highly responsive Sentinel-1 image polarization to water bodies[32]. So that it is easy to distinguish between water bodies and non-water bodies. Many other studies have used radar imagery, especially for Sentinel-1 to map water bodies [18], [22], [33], [34]

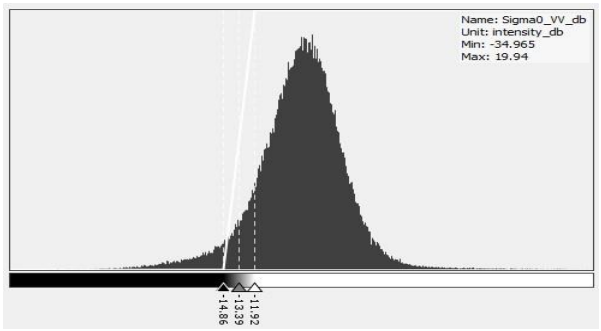

Fig. 4. Determination of boundary values between water bodies and non-water bodies in Sentinel-1 image

3.3 Land Cover Classification

Land cover classification using the Random Forest algorithm [20], [35] which is run on the SNAP program for processing Sentinel-2 data. Based on the results of the interpretation using TrueColor composites, 8 types of land cover were determined as shown in **Table 2**.

Table 2. Land Cover area classified using Sentinel-2

ID	Land Cover	Pixel Count	Areas (m^2)	Areas (Ha)
0	Cloud	1,919	191,900	191.9
1	Waterbodies	5,245	524,500	524.5
2	Built-up land	23,614	2,361,400	2,361.4

3	Cloud Shadow	2,089	208,900	208.9
4	Forest	46,463	4,646,300	4,646.3
5	Agriculture	15,730	1,573,000	1573
6	Shrub	57,132	5,713,200	5,713.2
7	Sand	1,122	112,200	112.2

The results of the classification using Sentinel-2 data with Bands 2, 3, 4, and 8 as reference Bands for classification input, can be seen in **Figure 5**. It can be seen that the distribution of land cover in the form of agriculture is spread in the western area, while for settlements it is spread along the Mata Allo River as the study location. Meanwhile, shrubs and forests are still quite extensive surrounding settlements and hills. The dominant land use is forest, followed by shrubs, agricultural land, and built-up land

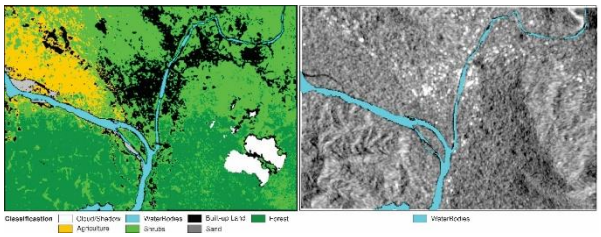

Fig. 5. LULC Classification Extraction from Sentinel-2 (Band 2,3,4 and 8) Imagery (left), Waterbodies Extraction from Sentinel-1 VV Polarization (right)

3.4 . Accuracy of Classification and Waterbodies Extraction

Testing the accuracy of classification and identification of water bodies using the Confusion Matrix/Error Matrix method with Kappa Hat Coefficient. The results of the classification using sentinel-2 data with the Random Forest algorithm of **82.9%** with a Kappa Hat Coefficient of **0.80**. As for the results of the extraction of water bodies using Sentinel-1 data with the determination of the threshold value, the mapping obtained is as large as compared to High-Resolution Image from Google Earth **89.6%** with Kappa Hat Coefficient **0.81**.

3.5 Flood Modelling

Flood modeling with the HEC-RAS program, utilizing Terrain data formed from 8.2m resolution DEM data. As well as inputting river discharge data from the results of field measurements. Field measurements by a discharge measuring device installed by the Enrekang Regency Government in the Mata Allo River. The maximum discharge at the time of the flood incident was 73.23m^3/s at 12:00 PM on 29 April 2019. And the normal discharge was 8.49m^3/s at 12:00PM on 28 April 2019 around the upstream of the modeling as shown in **Figure 7**. As for 12:00 AM on 29 April 2019 based on the recording of the river flow rate of 64.74m^3/s. This means that there is a drastic increase in discharge (6-8 times) from normal discharge.

Fig. 6. Floods in Enrekang District (source: tribunnews.com)

If we look at the water level rise in the simulation and modeling data based on the measurement discharge data (**Table 3**). From normal discharge to maximum discharge, there was an increase in water level of 4.63m. If adjusted to the height of the river embankment at the study site. Such a large increase in water level can cause flooding in residential areas as shown in **Figure 6**. Based on reports from the National Disaster Management Agency and reports from the Public Health Crisis Center of the Ministry of Health of the Republic of Indonesia. The water level rise started around 04.00 AM on 29 April 2019. Very high intensity of rainfall [36], [37] and due to changes in land use in upstream areas [8], [38] become one of the factors causing flooding in the study area. To see the flow characteristics of each cross-section formed, see **Appendix 1**.

Table 3. River Water Level on Cross Section 744 (through the affected city)

Date	Time	Q Total (m^3/s)	Min Channel Elevation (masl)	Water Surface Elevation (masl)
29-Apr-19	00:00	8.49	41.91	46.45
29-Apr-19	06:00	29.14	41.91	48.65
29-Apr-19	18:00	57.05	41.91	50.96
29-Apr-19	24:00	67.08	41.91	51.08

Figure 7 below shows the condition of the cross-section of the river in the upstream part of the study river and the downstream area of the study river which is located in the urban area of Enrekang Regency. You can see the difference in water level when viewed from Bank Level. The bank-level shows the river boundary if its height is crossed by the water level, it is included in the overflow class [16], [39]. At maximum discharge conditions, almost all areas on the right and left of the river experience overflow. Apart from rainfall intensity, land use changes, are based on existing river cross-sectional models. This cross-section is included in the small category to accommodate the existing river flow when compared to the cross-sectional area of the Saddang River which is to the west of the Mata Allo River. In addition, the slopes in the upper reaches of the

Mata Allo River have included slopes that cause water accumulation to accelerate [40].

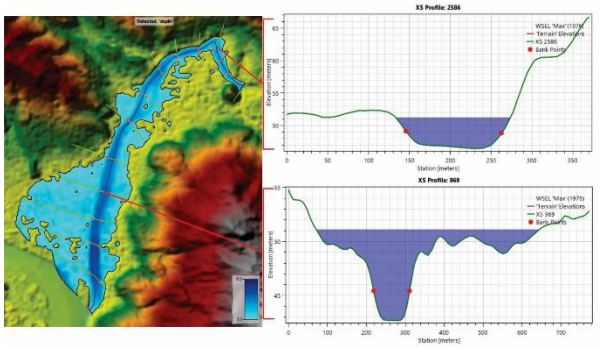

Fig. 7. Cross Section around upstream and downstream sectors of the study area

Figure 8 below shows the difference in runoff conditions during normal discharge conditions and at maximum discharge conditions that cause flooding. It can be seen that the runoff area is quite wide in the western area of the Mata Allo River. The location of the overflow is the city of Enrekang which always experiences flooding [2].

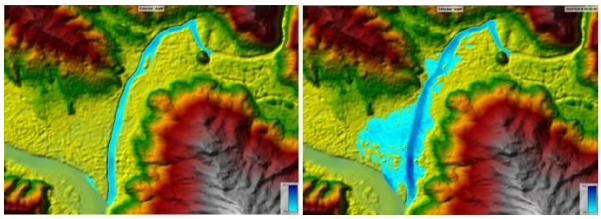

Fig. 8. Flow conditions at normal discharge (8.49m^3/s) (left) and maximum discharge (flood) (73.23m^3/s) (right)

3.6 Flood Affected Area

Based on the results of land cover analysis using Sentinel-2 data and extraction of water bodies from Sentinel-1 data, as well as flood area simulations using DEM discharge and Terrain data. Then the results of the analysis of areas affected by flooding in Juppandang District, Enrekang Regency are obtained as presented in **Figure 9**.

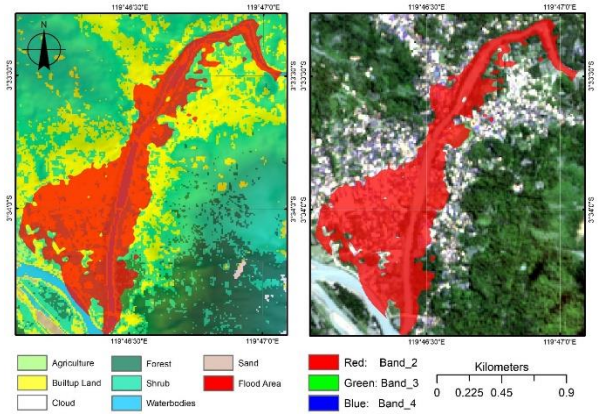

Fig. 9. Flood Affected Area of Mata Allo River 29 April 2019

It was found that the most affected areas related to human activities and people's livelihoods were built-up areas which reached 47.26ha of the affected area. Followed by agricultural land of 1,184Ha, while Shrub of 27.09Ha which can be connected to plantation land. The total area of the flooded area is 87.66 ha. More details can be seen in **Table 4** below.

Table 4. Types of Land Use Areas Affected by the Flood

No.	LULC	Affected Area (ha)
1	Agriculture	1.184
2	Built-up Land	47.260
3	Cloud(shrub)	0.146
4	Forest	1.957
5	Sand	0.129
6	Shrub	27.009
7	Waterbodies	9.974
	Total	**87.659**

The results from the affected areas are not much different from the results of flood event reports issued by the local government, such as from the National Disaster Management Agency. As for the accuracy of simulation and modeling results, it cannot be done accurately due to past flood events, and there are no reports on the related water level. However, it can be adjusted with the results of interviews from several sources of affected residents.

4 Conclusion

Based on the analysis results obtained, the use of an integrated approach between sentinel-2 and sentinel-1 images on the results of flood modeling or simulation with the HEC-RAS program is very possible and helps provide additional information. However, to produce better mapping accuracy, it is better to have the availability of hourly discharge data so that there are no data input errors. In addition, with the simulation results and flood modeling, it is hoped that the government can move to overcome this problem. And for future research to input more complete simulation and modeling data, such as sedimentation conditions, amount of rainfall, and other parameters.

References

1. M. A. Widiawaty and M. Dede, “Pemodelan Spasial Bahaya Dan Kerentanan Bencana Banjir Di Wilayah Timur Kabupaten Cirebon,” *J. Dialog Penanggulangan Bencana*, vol. **9**, no. 2, pp. 142–153, 2018.
2. BNPB, “Data Informasi Bencana Indonesia (DIBI),” Jakarta Timur, 2019. [Online]. Available: https://dibi.bnpb.go.id/xdibi/read/31156/73/16//2019/04/2//2
3. G. D. Bathrellos, H. D. Skilodimou, K. Chousianitis, A. M. Youssef, and B. Pradhan, “Suitability estimation for urban development using multi-hazard assessment map,” *Sci. Total Environ.*, vol. **575**, pp. 119–134, 2017, doi: 10.1016/j.scitotenv.2016.10.025.

4. A. Ezzine, S. Saidi, T. Hermassi, I. Kammessi, F. Darragi, and H. Rajhi, "Flood mapping using hydraulic modeling and Sentinel-1 image: A case study of Medjerda Basin, northern Tunisia," *Egypt. J. Remote Sens. Sp. Sci.*, vol. **23**, no. 3, pp. 303–310, 2020, doi: 10.1016/j.ejrs.2020.03.001.
5. B. K. Tjasyono, I. Juaeni, and W. B. Harijono, "Proses Meteorologis Bencana Banjir," *J. Meteorol. dan Geofis.*, vol. **8**, no. 2, pp. 64–78, 2007.
6. D. Suryanto, *Tanah Airku Salah Kelola Hujan*. Yogyakarta: Deepbulish, 2016.
7. S. Wulandarie, "Integrasi Sig-Infoworks River Simulation Untuk Pemodelan Hidrodinamik Sungai Saddang Dan Sungai Mata Allo," *J. Environ. Sci.*, vol. **2**, no. 2, p. 178, 2020, doi: 10.35580/jes.v2i2.13331.
8. H. Rachmayanti, R. Musa, and A. Mallombasi, "Studi Pengaruh Perubahan Tata Guna Lahan Terhadap Debit Banjir Dengan Menggunakan Software HEC HMS (Studi Kasus DAS Saddang)," vol. **01**, no. 01, pp. 1–9, 2022.
9. T. Cahyono, M. P. Hadi, and D. Mardianto, "Pemodelan Spasial untuk Pembuatan Peta Rawan Banjir dan Peta Tingkat Risiko Banjir Bengawan Solo di Kota Surakarta," *Maj. Geogr. Indones.*, vol. **29**, no. 1, p. 32, 2015, doi: https://doi.org/10.22146/mgi.13102.
10. N. A. Haris, S. S. Kusuma, S. Arjasakusuma, and P. Wicaksono, "Comparison of Sentinel-2 and Multitemporal Sentinel-1 SAR Imagery for Mapping Aquaculture Pond Distribution in the Coastal Region of Brebes Regency, Central Java, Indonesia," *Geogr. Tech.*, vol. **16**, no. Special Issue, pp. 128–137, 2021, doi: 10.21163/GT_2021.163.10.
11. B. Haack and M. Bechdol, "Integrating multisensor data and RADAR texture measures for land cover mapping," *Comput. Geosci.*, vol. **26**, no. 4, pp. 411–421, 2000, doi: 10.1016/S0098-3004(99)00121-1.
12. N. D. Herold, B. N. Haack, and E. Solomon, "An evaluation of radar texture for land use/cover extraction in varied landscapes," *Int. J. Appl. Earth Obs. Geoinf.*, vol. **5**, no. 2, pp. 113–128, 2004, doi: 10.1016/j.jag.2004.01.005.
13. S. Chen, J. Useya, and H. Mugiyo, "Decision-level fusion of Sentinel-1 SAR and Landsat 8 OLI texture features for crop discrimination and classification: case of Masvingo, Zimbabwe," *Heliyon*, vol. **6**, no. 11, p. e05358, 2020, doi: 10.1016/j.heliyon.2020.e05358.
14. I. A. El-Magd, E. Hermas, and M. El Bastawesy, "GIS-modelling of the spatial variability of flash flood hazard in Abu Dabbab catchment, Red Sea Region, Egypt," *Egypt. J. Remote Sens. Sp. Sci.*, vol. **13**, no. 1, pp. 81–88, 2010, doi: 10.1016/j.ejrs.2010.07.010.
15. R. Cheah, L. Billa, A. Chan, F. Y. Teo, B. Pradhan, and A. M. Alamri, "Geospatial modeling of watershed peak flood discharge in Selangor, Malaysia," *Water (Switzerland)*, vol. **11**, no. 12, pp. 1–12, 2019, doi: 10.3390/w11122490.
16. A. Tegos, A. Ziogas, V. Bellos, and A. Tzimas, "Forensic Hydrology: A Complete Reconstruction of an Extreme Flood Event in Data-Scarce Area," *Hydrology*, vol. **9**, no. 5, p. 93, 2022, doi: 10.3390/hydrology9050093.
17. J. T. Samarasinghe, V. Basnayaka, M. B. Gunathilake, H. M. Azamathulla, and U. Rathnayake, "Comparing Combined 1D/2D and 2D Hydraulic Simulations Using High-Resolution Topographic Data: Examples from Sri Lanka—Lower Kelani River Basin," *Hydrology*, vol. **9**, no. 2, pp. 1–17, 2022, doi: 10.3390/hydrology9020039.
18. V. K. Rana and T. M. V. Suryanarayana, "Evaluation of SAR speckle filter technique for inundation mapping," *Remote Sens. Appl. Soc. Environ.*, vol. **16**, no. October, p. 100271, 2019, doi: 10.1016/j.rsase.2019.100271.
19. P. O. Gislason, J. A. Benediktsson, and J. R. Sveinsson, "Random forests for land cover classification," *Pattern Recognit. Lett.*, vol. **27**, no. 4, pp. 294–300, 2006, doi: 10.1016/j.patrec.2005.08.011.
20. A. D. Kulkarni and B. Lowe, "Random Forest Algorithm for Land Cover Classification," *Int. J. Recent Innov. Trends Comput. Commun.*, vol. **4**, no. 3, pp. 58–63, 2016, [Online]. Available: https://scholarworks.uttyler.edu/cgi/viewcontent.cgi?article=1002&context=compsci_fac
21. S. Rapinel, E. Fabre, S. Dufour, D. Arvor, C. Mony, and L. Hubert-Moy, "Mapping potential, existing and efficient wetlands using free remote sensing data," *J. Environ. Manage.*, vol. **247**, no. November 2018, pp. 829–839, 2019, doi: 10.1016/j.jenvman.2019.06.098.
22. C. B. Obida, G. A. Blackburn, J. D. Whyatt, and K. T. Semple, "River network delineation from Sentinel-1 SAR data," *Int. J. Appl. Earth Obs. Geoinf.*, vol. **83**, no. June, p. 101910, 2019, doi: 10.1016/j.jag.2019.101910.
23. A. Hardy *et al.*, "Automatic detection of open and vegetated water bodies using Sentinel 1 to map African malaria vector mosquito breeding habitats," *Remote Sens.*, vol. **11**, no. 5, 2019, doi: 10.3390/rs11050593.
24. M. Ottinger, K. Clauss, J. Huth, C. Eisfelder, P. Leinenkugel, and C. Kuenzer, "Time series sentinel-1 SAR data for the mapping of aquaculture ponds in coastal Asia," *Int. Geosci. Remote Sens. Symp.*, vol. **2018**-July, pp. 9371–9374, 2018, doi: 10.1109/IGARSS.2018.8651419.
25. S. Manfreda, M. Di Leo, and A. Sole, "Detection of Flood-Prone Areas Using Digital Elevation Models," *J. Hydrol. Eng.*, vol. **16**, no. 10, pp. 781–790, 2011, doi: 10.1061/(asce)he.1943-5584.0000367.
26. F. Bioresita, A. Puissant, A. Stumpf, and J. P. Malet, "Fusion of Sentinel-1 and Sentinel-2 image

time series for permanent and temporary surface water mapping," *Int. J. Remote Sens.*, vol. **40**, no. 23, pp. 9026–9049, 2019, doi: 10.1080/01431161.2019.1624869.

27. M. Haq, M. Akhtar, S. Muhammad, S. Paras, and J. Rahmatullah, "Techniques of Remote Sensing and GIS for flood monitoring and damage assessment: A case study of Sindh province, Pakistan," *Egypt. J. Remote Sens. Sp. Sci.*, vol. **15**, no. 2, pp. 135–141, 2012, doi: 10.1016/j.ejrs.2012.07.002.
28. S. Tian, X. Zhang, J. Tian, and Q. Sun, "Random forest classification of wetland landcovers from multi-sensor data in the arid region of Xinjiang, China," *Remote Sens.*, vol. **8**, no. 11, pp. 1–14, 2016, doi: 10.3390/rs8110954.
29. Gond V., E. Bartholomé, F. Ouattara, A. Nonguierma, and L. Bado, "Mapping and monitoring small ponds in dryland with VEGETATION instrument-----application to West Africa," *Proceeding Veg.*, no. April, pp. 327–333, 2000.
30. J. V. Soares, C. D. Rennó, A. R. Formaggio, C. D. C. F. Yanasse, and A. C. Frery, "An investigation of the selection of texture features for crop discrimination using SAR imagery," *Remote Sens. Environ.*, vol. **59**, no. 2, pp. 234–247, 1997, doi: 10.1016/S0034-4257(96)00156-3.
31. V. Demir and O. Kisi, "Flood Hazard Mapping by Using Geographic Information System and Hydraulic Model: Mert River, Samsun, Turkey," *Adv. Meteorol.*, vol. 2016, 2016, doi: 10.1155/2016/4891015.
32. H. W. Chung, C. C. Liu, I. F. Cheng, Y. R. Lee, and M. C. Shieh, "Rapid response to a typhoon-induced flood with an SAR-derived map of inundated areas: Case study and validation," *Remote Sens.*, vol. **7**, no. 9, pp. 11954–11973, 2015, doi: 10.3390/rs70911954.
33. B. Slagter, N.-E. Tsendbazar, A. Vollrath, and J. Reiche, "Mapping wetland characteristics using temporally dense Sentinel-1 and Sentinel-2 data: A case study in the St. Lucia wetlands, South Africa," *Int. J. Appl. Earth Obs. Geoinf.*, vol. **86**, no. October 2019, p. 102009, 2020, doi: 10.1016/j.jag.2019.102009.
34. Z. Zeng *et al.*, "Towards high resolution flood monitoring: An integrated methodology using passive microwave brightness temperatures and Sentinel synthetic aperture radar imagery," *J. Hydrol.*, vol. **582**, no. November 2019, p. 124377, 2020, doi: 10.1016/j.jhydrol.2019.124377.
35. G. Brandon and B. Bradley, "Classification Algorithms - Random Forest Working of Random Forest Algorithm," *Mach. Learn.*, vol. **3**, pp. 1–5, 2020.
36. S. A. Mohamed, "Application of satellite image processing and GIS-Spatial modeling for mapping urban areas prone to flash floods in Qena governorate, Egypt," *J. African Earth Sci.*, vol. **158**, no. March, p. 103507, 2019, doi: 10.1016/j.jafrearsci.2019.05.015.
37. J. S. Cabrera and H. S. Lee, "Flood-prone area assessment using GIS-based multi-criteria analysis: A case study in Davao Oriental, Philippines," *Water (Switzerland)*, vol. **11**, no. 11, 2019, doi: 10.3390/w11112203.
38. N. Machineni, V. S. P. Sinha, P. Singh, and N. T. Reddy, "The impact of distributed landuse information in hydrodynamic model application in storm surge inundation," *Estuar. Coast. Shelf Sci.*, vol. **231**, no. September, p. 106466, 2019, doi: 10.1016/j.ecss.2019.106466.
39. T. Nharo, H. Makurira, and W. Gumindoga, "Mapping floods in the middle Zambezi Basin using earth observation and hydrological modeling techniques," *Phys. Chem. Earth*, vol. **114**, no. June, p. 102787, 2019, doi: 10.1016/j.pce.2019.06.002.
40. A. N. Matori, D. U. Lawal, K. W. Yusof, M. A. Hashim, and A. L. Balogun, "Spatial analytic hierarchy process model for flood forecasting: An integrated approach," *IOP Conf. Ser. Earth Environ. Sci.*, vol. **20**, no. 1, 2014, doi: 10.1088/1755-1315/20/1/012029.

Appendix

Appendix 1. Flow characteristics in each cross section in 3 discharge models

River Sta	Profile	Q Total (m3/s)	Min Ch El (m)	W.S. Elev (m)	Crit W.S. (m)	E.G. Elev (m)	E.G. Slope (m/m)	Vel Chnl (m/s)	Flow Area (m2)	Top Width (m)	Froude # Chl
2999	Max WS	73.23	46.18	51.35		51.35	0.000126	0.23	340.44	87.54	0.03
2999	29APR2019 0000	8.49	46.18	50.46		50.46	0.000004	0.03	264.99	81.9	0.01
2999	29APR2019 1200	64.74	46.18	51.16		51.16	0.000115	0.22	323.56	86.35	0.03
2835	Max WS	73.2	46.11	51.31		51.32	0.000318	0.34	224.43	66.26	0.05
2835	29APR2019 0000	8.49	46.11	50.46		50.46	0.00001	0.05	170.85	59.53	0.01
2835	29APR2019 1200	64.52	46.11	51.12		51.12	0.000291	0.32	211.95	64.73	0.05
2720	Max WS	73.18	45.9	51.28		51.29	0.000193	0.29	286.03	87.51	0.04
2720	29APR2019 0000	8.49	45.9	50.46		50.46	0.000005	0.04	218.81	75.93	0.01
2720	29APR2019 1200	64.38	45.9	51.09		51.1	0.000175	0.26	269.85	84.48	0.04
2586	Max WS	73.15	46.47	51.27		51.27	0.000055	0.14	520.83	140.53	0.02
2586	29APR2019 0000	8.49	46.47	50.46		50.46	0.000002	0.02	410.14	132.28	0
2586	29APR2019 1200	64.14	46.47	51.08		51.08	0.00005	0.13	494.71	138.64	0.02
2414	Max WS	73.1	45.13	51.24		51.25	0.00021	0.33	275.05	105.58	0.05
2414	29APR2019 0000	8.49	45.13	50.46		50.46	0.000005	0.05	211.42	66.93	0.01
2414	29APR2019 1200	63.81	45.13	51.06		51.06	0.000186	0.3	256.38	97.45	0.04
2230	Max WS	73.05	46.48	51.2		51.2	0.000274	0.3	326.54	176.79	0.05
2230	29APR2019 0000	8.49	46.48	50.46		50.46	0.000011	0.05	208.86	146.11	0.01
2230	29APR2019 1200	63.45	46.48	51.02		51.02	0.000264	0.28	295.97	162.28	0.05
2053	Max WS	72.99	43.76	51.18		51.18	0.000024	0.13	610.82	164.58	0.02
2053	29APR2019 0000	8.49	43.76	50.45		50.45	0	0.02	526.93	105.96	0
2053	29APR2019 1200	63.1	43.76	51		51	0.00002	0.12	585.85	117.65	0.01
1818	Max WS	72.89	45.56	51.17		51.17	0.000063	0.16	615.4	282.97	0.02
1818	29APR2019 0000	8.49	45.56	50.45		50.45	0.000002	0.03	428.55	245.98	0
1818	29APR2019 1200	62.46	45.56	50.99		50.99	0.000057	0.15	566.04	271.21	0.02

1573	Max WS 29APR2019	72.75	44.67	51.15		51.15	0.000071	0.21	580.18	334.93	0.03
1573	0000 29APR2019	8.49	44.67	50.45		50.45	0.000002	0.03	377.88	225.79	0
1573	1200	61.48	44.67	50.97		50.97	0.000063	0.19	522.14	322.07	0.03
1240	Max WS 29APR2019	72.59	43.25	51.13		51.13	0.000019	0.12	725.69	200.86	0.01
1240	0000 29APR2019	8.49	43.25	50.45		50.45	0	0.02	597.77	167.35	0
1240	1200	60.34	43.25	50.96		50.96	0.000015	0.1	691.49	194.09	0.01
969	Max WS 29APR2019	72.42	42.69	51.13		51.13	0.000006	0.07	1515.17	574.7	0.01
969	0000 29APR2019	8.49	42.69	50.45		50.45	0	0.01	1137.22	527.32	0
969	1200	59	42.69	50.96		50.96	0.000005	0.06	1416.59	566.21	0.01
744	Max WS 29APR2019	72.16	41.91	51.13		51.13	0.000003	0.06	2185.7	775.37	0.01
744	0000 29APR2019	8.49	41.91	50.45		50.45	0	0.01	1668.16	731.66	0
744	1200	57.05	41.91	50.96		50.96	0.000002	0.05	2052.26	771.54	0.01
549	Max WS 29APR2019	71.93	39.49	51.13		51.13	0.000003	0.07	1624.13	625.9	0.01
549	0000 29APR2019	8.49	39.49	50.45		50.45	0	0.01	1258.26	446.95	0
549	1200	55.36	39.49	50.96		50.96	0.000002	0.05	1519.11	585.68	0.01
292	Max WS 29APR2019	71.67	40.7	51.13		51.13	0.000002	0.05	2175.99	536.1	0
292	0000 29APR2019	8.49	40.7	50.45		50.45	0	0.01	1815.03	531.37	0
292	1200	53.53	40.7	50.96		50.96	0.000001	0.04	2083.77	534.86	0
3	Max WS 29APR2019	71.53	41.39	42.45	42.16	42.59	0.060429	1.6	44.57	54.38	0.57
3	0000 29APR2019	8.49	41.39	41.75	41.63	41.78	0.060118	0.77	11.03	40.39	0.47
3	1200	52.45	41.39	42.29	42.03	42.4	0.063093	1.47	35.64	51.16	0.56